Acta Geochim (2024) 43:707–718
https://doi.org/10.1007/s11631-024-00693-3

ORIGINAL ARTICLE

Metamorphic P–T conditions and ages of garnet-biotite schists in the Dahongshan Group from the southwestern Yangtze Block

Jun-xiao Ma[1] · Guang-shu Yang[1] · Yong-feng Yan[1] · Xiao-Fei Xu[1] · Yun-hua Ren[2] · Hui Zhao[1] · Xiao-jun Zheng[1,3] · Yuan Qin[1]

Received: 17 December 2023 / Revised: 20 March 2024 / Accepted: 2 April 2024 / Published online: 5 May 2024

Abstract The Dahongshan Group, situated at the southwestern margin of the Yangtze Block, represents a geological unit characterized by relatively high-grade metamorphism in the region. This paper investigates the garnet-biotite schist from the Laochanghe Formation of the Dahongshan Group, employing an integrated approach that includes petrological analysis, phase equilibrium modeling, and zircon U–Pb dating. The schist is mainly composed of garnet, biotite, plagioclase, quartz, rutile, and ilmenite. Phase equilibrium modeling revealed the peak metamorphic conditions of 8–9 kbar and 635–675 °C. By further integrating the prograde metamorphic profile of garnet and geothermobarometric results, a clockwise *P–T* metamorphic evolution path is constructed, which includes an increase in temperature and pressure during the prograde stage. LA–ICP–MS zircon U–Pb dating and zircon Ti thermometry constrains the post-peak metamorphic age of 831.2 ± 7.2 Ma. Integrated with previously reported results, it is revealed that the southwestern margin of the Yangtze Block experienced a large-scale regional metamorphism during the Neoproterozoic (890–750 Ma), which is related to the collisional orogenic process. This may be associated with the late-stage assembly of the Rodinia supercontinent or with local compression and subduction processes during the breakup of the Rodinia supercontinent.

Keywords Southwestern Yangtze Block · Dahongshan Group · Phase equilibrium modeling · Zircon U–Pb dating · Neoproterozoic metamorphism

1 Introduction

The Precambrian crystalline basement along the western margin of the Yangtze Block, commonly known as the "Kangdian Axis", is closely aligned with the Sanjiang Orogenic Belt in the southwest. The region was traditionally conceptualized as exhibiting a dual-layered structure, characterized by a foundational Paleoproterozoic-Archean crystalline basement overlain by a Neoproterozoic folded basement of low-grade metamorphism. Subsequent research, however, has predominantly identified this basement as being largely constituted of Neoproterozoic (850–750 Ma) magmatic complexes (Zhou et al. 2002; Chen et al. 2005; Liu et al. 2005; Xiao et al. 2007; Wang et al. 2007; Geng et al. 2008; Huang et al. 2008; Zhu et al. 2008; Du et al. 2013). The southwestern margin of the Yangtze Block is characterized by an array of metamorphic rock series, with varying metamorphic grades, notably including the Dahongshan, Hekou, Dongchuan Groups, and Tong'an Formation (Yan 1981; Qian and Shen 1990; Geng et al. 2017). Over the past decades, three kinds of geodynamic mechanisms have been proposed for the southwestern margin of the Yangtze Block, including the orogenic belt model (Munteanu et al. 2010; Li et al. 2021, 2022), subduction model (Zhou et al. 2002; Chen et al. 2005; Xiao et al. 2007; Du et al. 2013)

Supplementary Information The online version contains supplementary material available at https://doi.org/10.1007/s11631-024-00693-3.

✉ Yong-feng Yan
yyf701018@sina.com

✉ Xiao-Fei Xu
xuxiaofei@kust.edu.cn

[1] Faculty of Land Resources Engineering, Kunming University of Science and Technology, Kunming 650093, China

[2] Geological Team 306 of Yunnan Non-Ferrous Metals Geological Bureau, Kunming 650217, China

[3] Yunnan Provincial Bureau of Non-Ferrous Geology, Kunming 650051, China

and mantle plume model (Li et al. 2003; Wang et al. 2007; Huang et al. 2008; Zhu et al. 2008). The extensive metamorphic rocks within the Precambrian crystalline basement (such as the Dahongshan and Hekou Groups) in the southwestern margin of the Yangtze Block serve as important carriers for unraveling the Neoproterozoic tectonic environment because these rocks can provide valuable information about the temperature, pressure, and timing of geological events.

The Dahongshan Group, situated on the southern flank of the Yangtze Block's southwestern margin, represents a geological unit distinguished by its relatively high-grade metamorphism within the western Yangtze Block. Stratigraphically, this group is subdivided into five formations from bottom to top: the Laochanghe, Manganghe, Hongshan, Feiweihe, and Potou Formations, predominantly comprising feldspar quartzite, garnet mica schist, marble, and garnet amphibolite (Qian and Shen 1990). The metamorphic ages of the Dahongshan Group range from 897 to 706 Ma (Cao et al. 1997; Greentree et al. 2006; Yang et al. 2012, 2013). Greentree et al. (2006) proposed that the metamorphic ages ranging from 860 to 820 Ma represent the ages of cooling, whereas Yang et al. (2012, 2013) interpreted the ages of 850–837 Ma as indicative of peak ages of the metamorphism. It is widely accepted that the metamorphic grade of the Dahongshan Group was confined to the lower amphibolite facies (Yan 1981; Qian and Shen 1990; Geng et al. 2017). However, the characteristics of zircons in the garnet-plagioclase-amphibolites of the Laochanghe Formation (exhibiting rounded, patchy, or structureless features; Yang et al. 2012) may indicate metamorphic grade reaching the upper-amphibolite to granulite facies. The current limited insight into the metamorphic conditions and timing within this region hinders the comprehension of the genesis mechanisms and associated tectonic background of the metamorphic processes.

In this study, we have concentrated on the garnet-biotite schist from the Laochanghe Formation, situated about 40 km southwest of Xinping County, as our primary subject. A comprehensive suite of methods, including detailed petrology, metamorphic phase equilibrium modeling, geothermobarometer, and zircon U–Pb dating, has been employed. The findings from this study have distinctly elucidated the metamorphic conditions and ages recorded by these rocks. This contributes significantly to our understanding of the regional tectonic evolution at the southwestern margin of the Yangtze Block.

2 Geological setting

The Yangtze Craton, a Neoproterozoic craton, was formed through the amalgamation of the Yangtze and Cathaysia Blocks along the Jiangnan Orogenic Belt during the period of 0.9–0.83 Ga (Zhang et al. 2013; Zhao 2015; Geng et al. 2015). The Yangtze Block, situated in the northwestern part of the Yangtze Craton, is separated from the North China Craton to the north by the Qinling-Dabie-Sulu orogenic belt, from the Songpan-Gantze Terrane in the northwest by the Longmenshan Fault, and from the Indochina Block in the southwest by the Jiangshan-Shaoxing Fault (Fig. 1A). The southwestern margin of the Yangtze Block is located within western Sichuan and central-northern Yunnan. It is a complex tectonic geological unit primarily composed of Neoproterozoic magmatic rocks, with some exposures of Paleoproterozoic metamorphic crystalline basement, such as Dahongshan, Dongchuan and Hekou Groups (Fig. 1B).

The Dahongshan Group is situated between the Yuanmou–Lüzhijiang Fault and the Ailao Mountain-Honghe Shear Zone. It is sporadically distributed on the surface areas of Xinping and Yuanjiang Counties within Yunnan, which is predominantly overlain by Tertiary and Jurassic sedimentary formations. The Dahongshan Group is divided into the Laochanghe, Manganghe, Hongshan, Feiweihe, and Potou Formations (Qian and Shen 1990) (Fig. 1C). The Laochanghe Formation is prominently exposed in the Laochanghe Valley and the Dibadu region to the northeast of the mining area. It is characterized by cross-bedded potassium feldspar quartzite and garnet mica schist. The Manganghe Formation is observable in both the Laochanghe and Manganghe valleys and their adjacent areas, consisting of greenschist, mica schist, sodium-rich metamorphic volcanic rocks, and marble. The Hongshan Formation, located in the eastern part of the mining area, predominantly consists of metamorphic volcanic breccia and tuff. The Feiweihe Formation, exposed on the northern side of the Feiweihe, is mainly composed of marble. The Potou Formation, situated southeast of the Dahongshan mining area, is primarily made up of garnet-biotite schist, quartzite, carbonaceous slate, and sericite schist.

Recent chronological studies have delineated the formation of the Dahongshan Group within the late Paleoproterozoic era, which corresponds temporally to the formation periods of the Dongchuan Group, Hekou Group, and Tong'an Formation (Greentree et al. 2006; Geng et al. 2012; Pang et al. 2015). Initially, the mica ^{40}Ar–^{39}Ar and whole-rock K–Ar dating from the Dahongshan Group revealed the ages ranging from 897 to 706 Ma (Cao et al. 1997; Greentree et al. 2006). Subsequent research by Yang et al. (2012, 2013) involved ^{40}Ar–^{39}Ar dating on muscovite and U–Pb dating on zircon from the garnet muscovite-plagioclase quartz schist and garnet-plagioclase amphibolite within the Laochanghe Formation, resulting in metamorphic ages of 850–837 Ma. In addition, earlier research posited that the Dahongshan Group predominantly experienced the greenschist- to lower amphibolite-facies metamorphism (Yan 1981; Qian

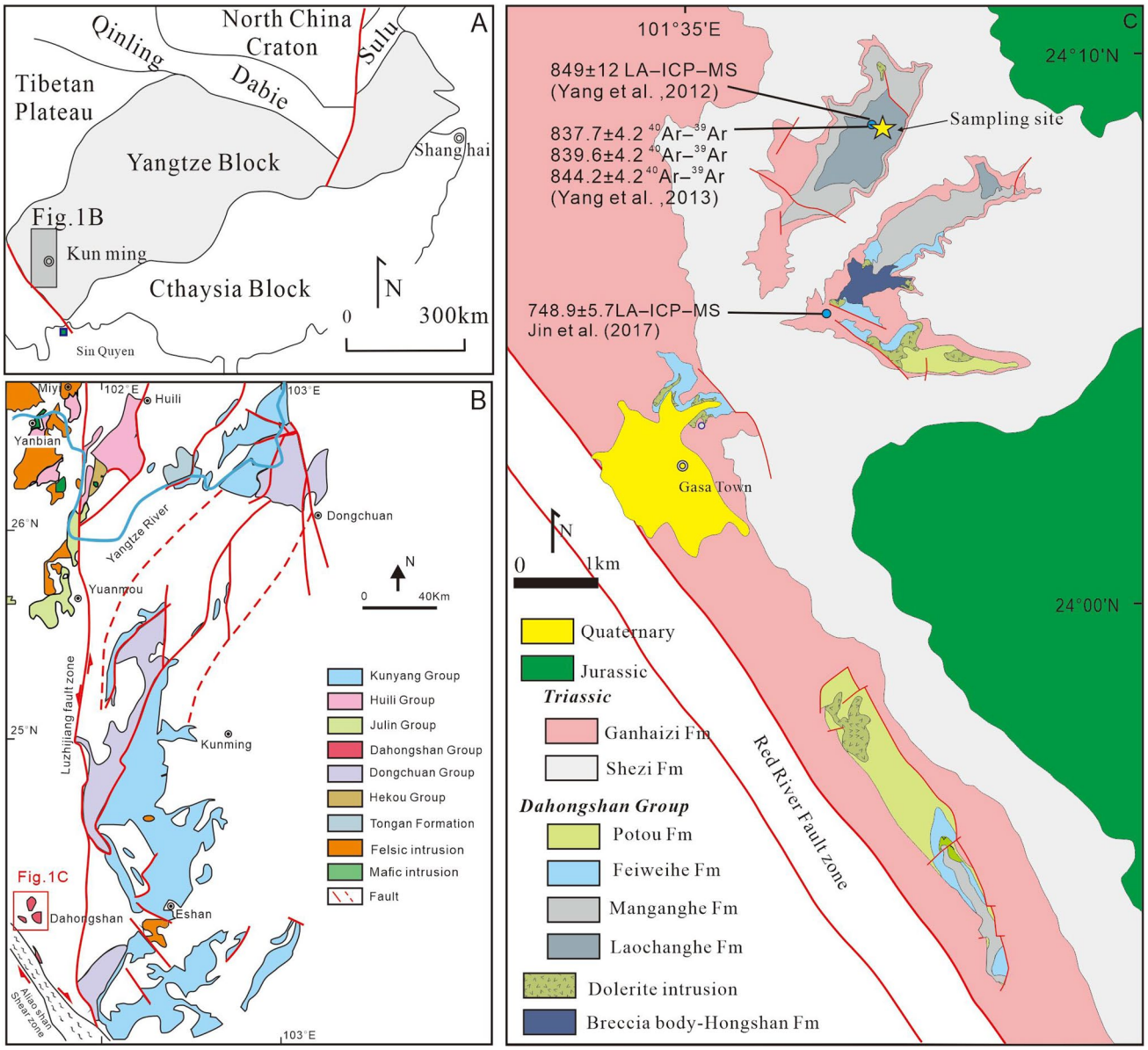

Fig. 1 **A** Simplified geotectonic map of the Yangtze block. **B** Simplified geologic map of the southwestern margin of the Yangtze Block. **C** Simplified geologic map of the Dahongshan Group

and Shen 1990). Cao (1997) provided a comprehensive overview of the metamorphic features of the Dahongshan rocks in the Nangan-Xilahé region, suggesting that the group underwent regional dynamothermal metamorphism during the Lüliang period and regional low-temperature dynamometamorphism during the Jinning period.

3 Petrology and mineral chemistry

Mineral compositions were analyzed using the JEOL JXA-8230 electron microprobe (EMP) at the Wuhan Shangpu Analytical Technology Co., Ltd. The operating conditions were 1–3 μm beam size, 15 kV acceleration voltage, and 20 nA beam current. Mineral abbreviations in this study follow Whitney and Evans (2010). Representative mineral

compositions and the mole fractions of end-members are listed in Supplementary Table S1.

The samples analyzed in this study were collected from the northeast-southwest trending Laochanghe River gully, located in the vicinity of Dahongshan, Xinping County, Yunnan Province (Fig. 1C), belonging to the Laochanghe Formation. The samples are garnet-biotite schist, which exhibits a gray-black color, and porphyroblastic garnet grains are also visible at the outcrop (Fig. 2A–B).

These samples are predominantly comprised of garnet (35%), biotite (40%), quartz (15%), and plagioclase (10%), along with minor accessory minerals including rutile, ilmenite, and zircon (Fig. 2D–F). The garnet porphyroblasts in these samples are present as subhedral porphyroblasts and display variable sizes with radii up to 6 mm. They are in contact with quartz, plagioclase, and biotite, and contain the inclusions of quartz and ilmenite (Fig. 2C–F). Biotite occurs as irregular flakes in the matrix, commonly hosting abundant rutile inclusions (Fig. 2E). Ilmenite occurs as mineral inclusions in garnet and biotite, while rutile is present in the matrix or as mineral inclusions in biotite. In addition, rutile has been partially replaced by ilmenite (Fig. 2E).

Garnet in the sample 22LC–8 is almandine- and grossular-rich (X_{Alm} = 0.61–0.75; X_{Grs} = 0.16–0.25) with low spessartine (X_{Sps} = 0.01–0.12) and pyrope (X_{Prp} = 0.02–0.10; Supplementary Table S1). The compositional zonation of the garnet grains displays pronounced variation from core to rim, marked by an increase in almandine and pyrope, and a decrease in spessartine. Conversely, grossular is relatively flat in the core but exhibits a rapid decrease close to the rim (Fig. 3). Biotite in the matrix that is not in contact with garnet (Bt_1) has similar X_{Mg} values (0.49–0.52) but lower Ti contents (0.08–0.12 cpfu) than those in contact with garnet (Bt_2; X_{Mg}: 0.51–0.54; Ti: 0.07–0.09 cpfu). The matrix plagioclase exhibits CaO contents and X_{An} values ranging

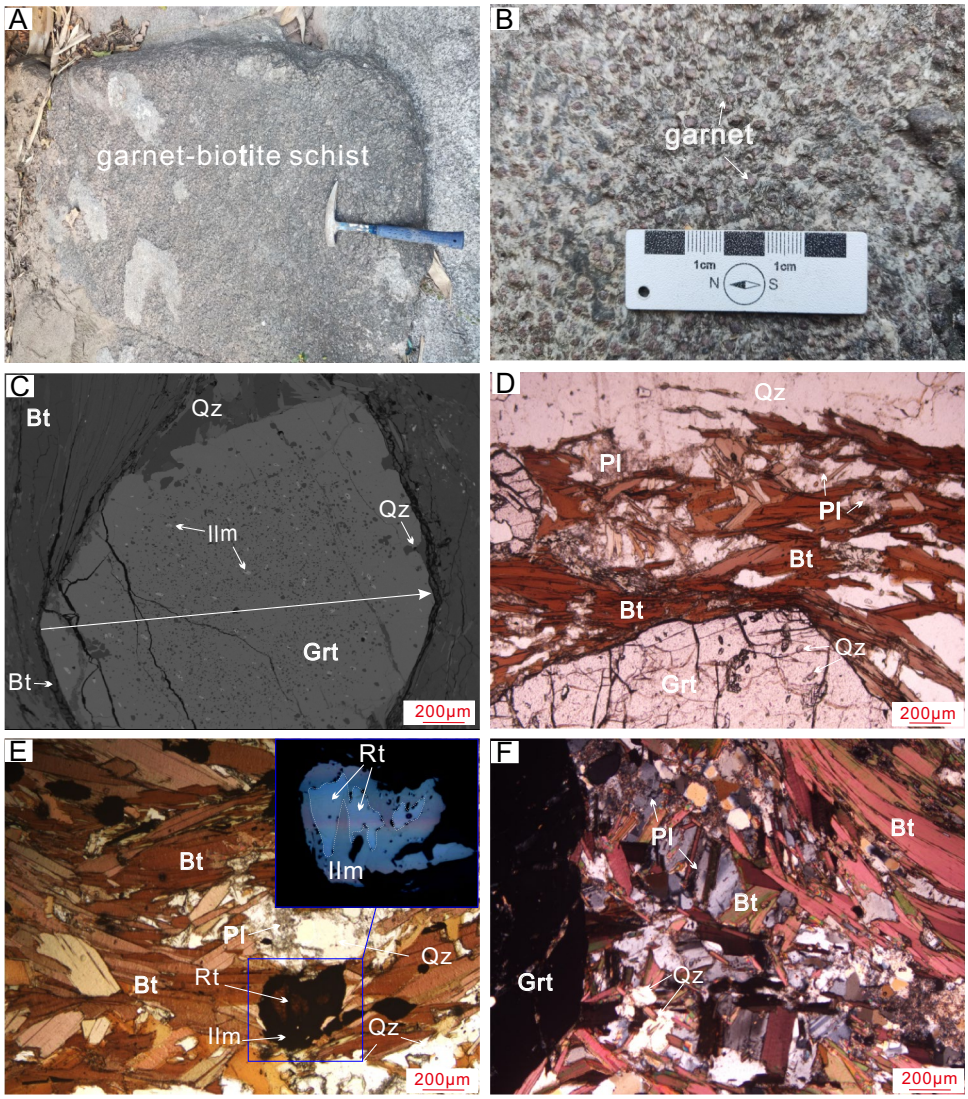

Fig. 2 Field and microscopic photographs of garnet-biotite schist from the Danhongshan Group. **A**–**B** Field photographs of garnet-biotite schist; **C**–**F** Photomicrographs showing the typical microstructure of the gaenet, biotite, plagioclase, quartz, rutile and ilmenite. The arrows show directions of rim–core–rim profiles analyzed by EMP as shown in ©

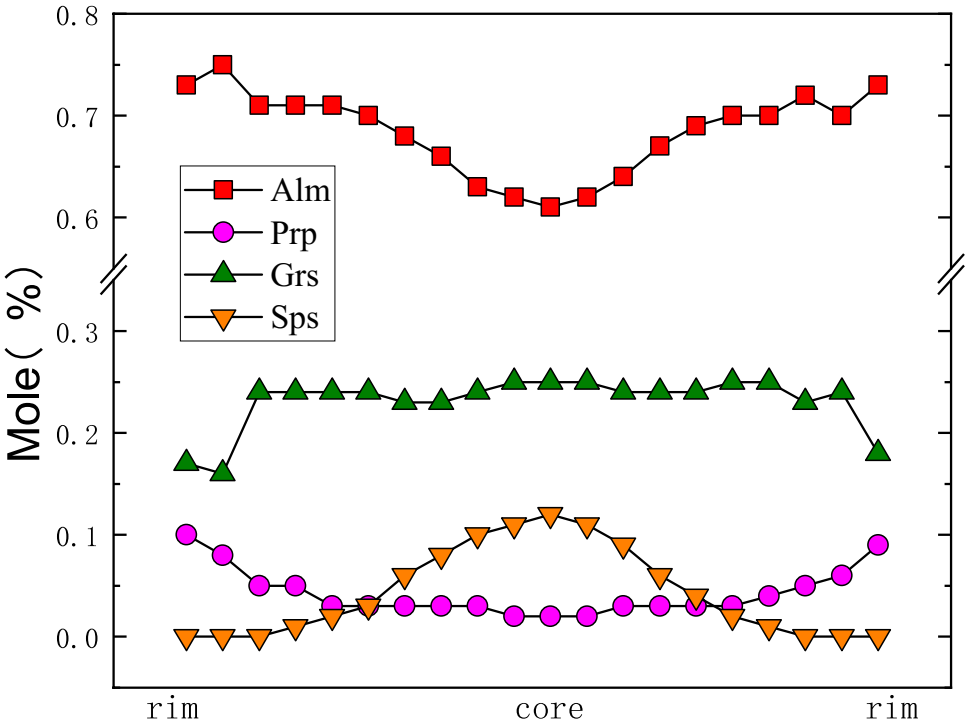

Fig. 3 Compositional Profile of Garnet from sample 22LC–8 along the profile as shown in Fig. 2C, showing the variation of the almandine (Alm), spessartine (Sps), pyrope (Prp), and grossular (Grs) from rim–core–rim

between 6.38wt%–7.05wt% and 0.31–0.38, respectively (Supplementary Table S1).

Metamorphic P–T conditions.

3.1 Phase equilibrium modeling

In this study, phase equilibrium modeling was conducted on the garnet-biotite schist (sample 22LC–8) using the GeoPS program version 3.4 (Xiang and Connolly 2022), in conjunction with the internally consistent thermodynamic dataset ds62 (Holland and Powell 1998, 2011). The MnO–Na_2O–CaO–K_2O–FeO–MgO–Al_2O_3–SiO_2–H_2O–TiO_2–Fe_2O_3 (MnNCKFMASHTO) system was selected to calculate *P–T* pseudosections. The re-parameterized activity-composition (a–x) models incorporated in this modeling including garnet, biotite, chlorite, orthopyroxene (White et al. 2014), feldspar (Holland and Powell 2003), and ilmenite (White and Powell 2002), along with pure end-member components for quartz, and rutile. H_2O was assumed to be in excess for the modeling, with oxygen content determined by $P–X_O$ diagrams. The mineral abbreviations follow Whitney and Evans (2010).

The bulk chemical compositions were determined by wavelength-dispersive X-ray fluorescence (XRF) spectrometry on a fused bead at the ALS Chemex in Guangzhou, China. The normalized molar proportions used for the phase equilibrium modeling are shown in Fig. 4.

The *P–T* pseudosection for sample 22LC–8 was calculated over a *P–T* window of 4–12 kbar and 450–750 °C, as illustrated in Fig. 4B. The solidus is predicted at temperatures between 650 °C and 750 °C in the range of modeled pressures (Fig. 4B). As shown in Fig. 4B and C the Ti isopleths in biotite, the X_{An} isopleths in plagioclase and the isopleths of X_{Sps}, X_{Grs}, and X_{Prp} in garnet are calculated. The Ti isopleths in biotite are nearly vertical and increase with rising temperature, while the X_{An} isopleths in plagioclase exhibit a moderate positive slope, decreasing with increasing pressure (Fig. 4B). The observed mineral assemblage in the sample is represented by a field of Grt + Bt + Pl + Rt + Ilm (+ Qz + H_2O), which occurs in the *P–T* ranges of 8–10 kbar and 600–690 °C (Fig. 4A). The measured X_{An} (0.31–0.38) of matrix plagioclase and the Ti content (0.08–0.12 cpfu) of Bt_1 further constrains the *P–T* range of the stage to be 8–9 kbar and 635–675 °C (Fig. 4B). Bt_2 has lower Ti content (0.07–0.09 cpfu) than Bt_1, this suggests that the Bt_2 formed later than Bt_1 and represents growth during the cooling stage. In addition, the garnet displays pronounced compositional zoning (is characterized by a decrease in spessartine and an increase in pyrope from core to rim, while the grossular is relatively flat in the core and significantly decreases at the rim), indicating that the zoning records the histories of the sample 22LC–8 during prograde stage (Spear 1993; Ague and Carlson 2013; Baxter et al. 2013; Caddick and Kohn 2013). However, the isopleths of X_{Sps}, X_{Grs}, and X_{Prp} in garnet cannot be used to define the prograde *P–T* conditions, which may be related to localized compositional domains during garnet growth. In contrast, the growth

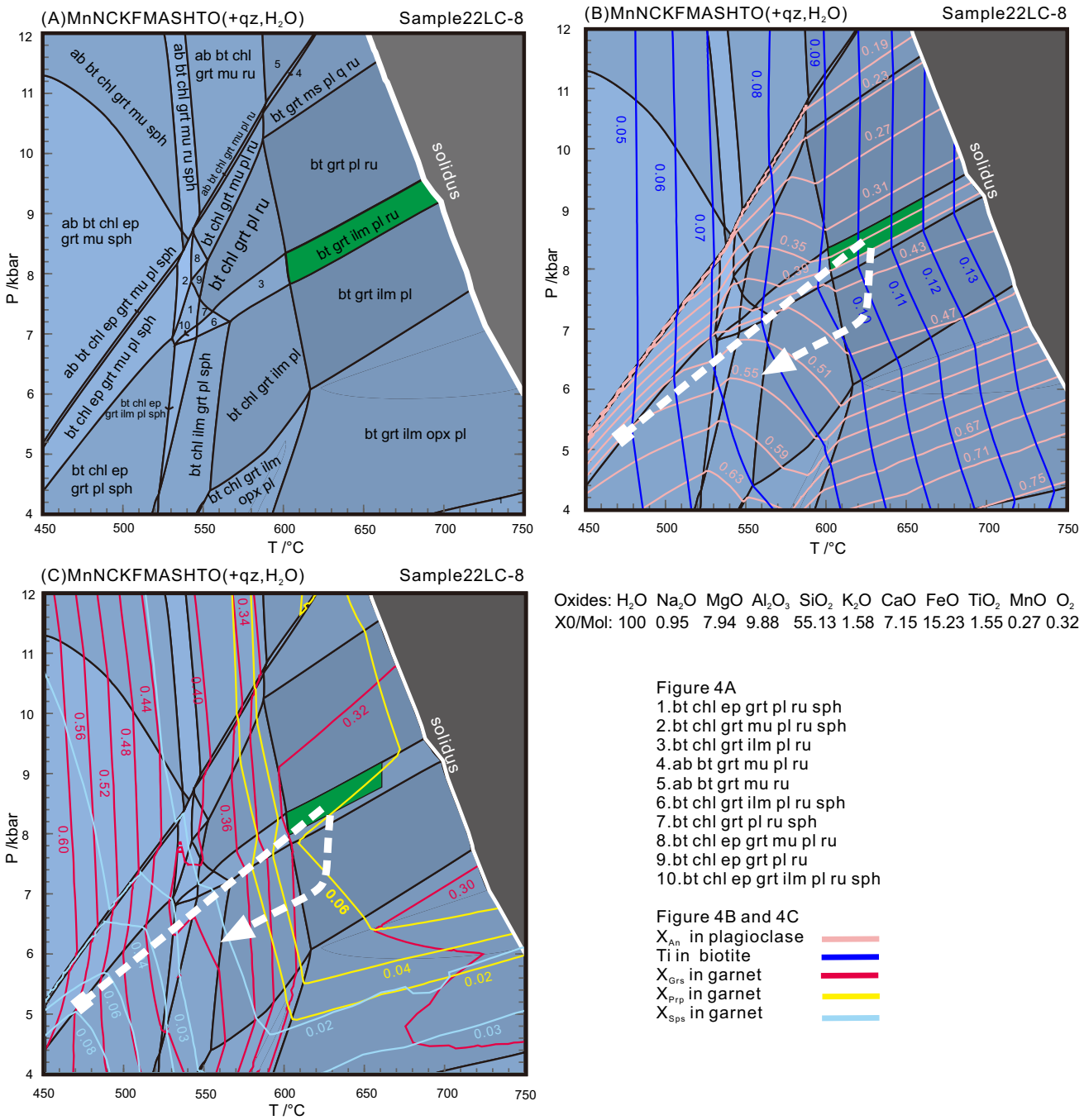

Fig. 4 P–T pseudosections for the sample 22LC–8. **A** P–T pseudosection; **B** P–T pseudosection with isopleths of the X_{An} in plagioclase and Ti in biotite; **C** P–T pseudosection with isopleths of the X_{Sps} X_{py} and X_{grs} in garnet.

conditions of garnet can be constrained by the changing trends of the compositional profile of garnet due to the same metamorphic reaction mechanism under the same conditions. As a result, a prograde metamorphic *P–T* path with heating and compression is defined for sample 22LC–8 on the basis of the changing trends of the X_{Sps}, X_{Grs} and X_{Prp} in garnet from core to rim (Fig. 4C).

3.2 Geothermobarometry

In this study, we applied the Ti-in-biotite geothermometer (Henry et al. 2005) and the garnet-biotite-plagioclase-quartz (GBPQ) geothermobarometer (Wu et al. 2004) to calculate the metamorphic *P–T* conditions of the garnet-biotite schist sample 22LC–8. The Ti-in-biotite geothermometer

has yielded metamorphic temperatures of 552–630 °C and 507–579 °C using the compositions of Bt_1 and Bt_2, respectively. The compositions of the garnet rims and Bt_2 were selected to calculate the *P–T* conditions by GBPQ geothermobarometer, because they are texturally in equilibrium. The results yielded metamorphic *P–T* conditions of 6.6–7.8 kbar and 539–570 °C.

4 Zircon U–Pb Geochronology

The zircon U–Pb dating and trace element analyses for the garnet-biotite schist sample 22LC–8 were carried out at the Wuhan Shangpu Analytical Technology Co., Ltd, using an Agilent 7900 inductively coupled plasma mass spectrometer (ICP-MS) instrument equipped with a GeoLas HD laser ablation system. Helium was used as the carrier gas to transport the ablated material. The laser spot was 24 μm in diameter, and a laser frequency of 5 Hz was used (Liu et al. 2008). The detailed analytical procedure has been described by Liu et al. (2010). An Excel-based software ICPMSDataCal 10.8 was used to perform off-line selection and integration of background and analyzed signals, time-drift correction, and quantitative calibration for trace element analysis and U–Pb dating (Liu et al. 2008, 2010). Concordia diagrams and weighted mean calculations were made using Isoplot 4.15 (Ludwig 2003). Details of the zircon U–Pb dating results are presented in Table 1.

Most zircon grains from the sample 22LC–8 are 80–130 μm in size with rounded to anhedral shapes (Fig. 5A–F). Some zircon grains display core-rim structures, characterized by inherited magmatic zircon cores and overgrowth metamorphic rims with varying widths, while other rounded zircons exhibit patchy or structureless appearances (Fig. 5A–F).

Sixteen spot analyses on 16 zircon grains of the sample 22LC–8 yielded variable contents of Th (0.5–21 ppm) and U (134–684 ppm), with low Th/U ratios of 0.01–0.05 (Table 1). Three analyses are discordant because of Pb loss (Fig. 5G), and the remaining 13 analyses are concordant and give a weighted mean $^{206}Pb/^{238}U$ age of 831.2 ± 7.2 Ma (N = 13, MSWD = 1.3; Fig. 5G). In a chondrite-normalized rare earth element (REE) variation diagram (Fig. 5H), the zircons display flat to depleted heavy rare earth elements (HREEs) pattern, without a pronounced Eu anomaly. In addition, after removing the data with abnormal Ti content in zircon, the remaining Ti content in zircon is 0.07–0.12 (Supplementary Table S2), and the temperatures deduced from the Ti-in-zircon thermometer range from 503 to 668 °C (Mean = 616 °C; Supplementary Table S2). The values of SiO_2 activity (αSiO_2) and TiO_2 activity (αTiO_2) were considered to be 1, as quartz and rutile are present in abundance in the sample 22LC–8.

Table 1 LA–ICP–MS zircon U–Pb data for samples 22LC-8 from the Dahongshan Complex

Spot	Content (ppm)				Isotope retios								Age (Ma)							
	Th	U	Th/U	Pb*	$^{207}Pb/^{206}Pb$	1σ	$^{207}Pb/^{235}U$	1σ	$^{206}Pb/^{238}U$	1σ	$^{208}Pb/^{232}Th$	1σ	$^{207}Pb/^{206}Pb$	1σ	$^{207}Pb/^{235}U$	1σ	$^{206}Pb/^{238}U$	1σ	$^{208}Pb/^{232}Th$	1σ
1	21.0	395	0.05	58.60	0.0694	0.0025	1.3477	0.0503	0.1394	0.0022	0.0215	0.0015	909	72.995	867	21.78332244	841	12.58252912	430	29.4855
2	2.71	448	0.01	67.30	0.0687	0.0022	1.3498	0.0420	0.1411	0.0016	0.0383	0.0033	900	60.185	867	18.14272162	851	9.140003073	759	63.93930747
3	0.50	137	0.00	20.31	0.0707	0.0037	1.3321	0.0667	0.1365	0.0019	0.1405	0.0724	948	108.185	860	29.03213824	825	10.88756428	2658	1283.212674
4	4.33	276	0.02	40.23	0.0692	0.0024	1.3113	0.0440	0.1363	0.0016	0.0593	0.0055	906	72.225	851	19.33539632	824	9.229102242	1164	104.6717142
5	4.87	289	0.02	42.23	0.0691	0.0023	1.3463	0.0441	0.1400	0.0020	0.0230	0.0028	902	68.5175	866	19.0754217	845	11.51162817	459	54.69006663
6	1.78	681	0.00	98.25	0.0671	0.0019	1.2894	0.0369	0.1377	0.0016	0.1275	0.0137	840	54.63	841	16.36052083	831	8.856082718	2425	245.5098399
7	13.7	684	0.02	100.08	0.0673	0.0021	1.2802	0.0389	0.1362	0.0016	0.0174	0.0023	848	70.525	837	17.32119939	823	8.808162085	349	46.29969839
8	0.66	134	0.00	20.14	0.0704	0.0030	1.3831	0.0579	0.1407	0.0019	0.1080	0.0180	943	85.6475	882	24.66123523	849	10.68134418	2072	329.0219476
9	4.18	413	0.01	58.60	0.0677	0.0026	1.2813	0.0516	0.1356	0.0019	0.0330	0.0040	857	80.395	837	22.98702106	820	10.91810469	655	77.49378513
10	0.68	179	0.00	25.58	0.0696	0.0026	1.3114	0.0512	0.1350	0.0020	0.1508	0.0246	917	77.78	851	22.49382428	816	11.15300026	2838	431.2094156
11	2.75	333	0.01	48.72	0.0665	0.0021	1.2758	0.0405	0.1381	0.0021	0.0395	0.0048	833	60.1825	835	18.06517711	834	11.81695937	783	93.89669458
12	16.4	453	0.04	58.94	0.0681	0.0025	1.2851	0.0582	0.1350	0.0035	0.1173	0.0338	872	75.9225	839	25.88771732	816	19.92210491	2242	612.1802105
13	2.96	274	0.01	38.28	0.0636	0.0024	1.1968	0.0468	0.1361	0.0019	0.0289	0.0044	731	76.845	799	21.65107021	822	10.52633737	575	86.89518827
14	15.6	263	0.06	37.60	0.0834	0.0034	1.4541	0.0584	0.1259	0.0017	0.3160	0.0404	1277	85.6475	912	24.17059668	765	9.526939552	5550	620.1012059
15	13.3	208	0.06	32.24	0.0843	0.0035	1.6286	0.0664	0.1386	0.0018	0.1109	0.0092	1302	79.63	981	25.66812538	837	10.3517905	2127	166.7437987
16	1.53	238	0.01	37.97	0.0660	0.0024	1.4031	0.0535	0.1528	0.0025	0.0435	0.0074	809	77.7725	890	22.59326062	917	13.72674407	860	143.3875059

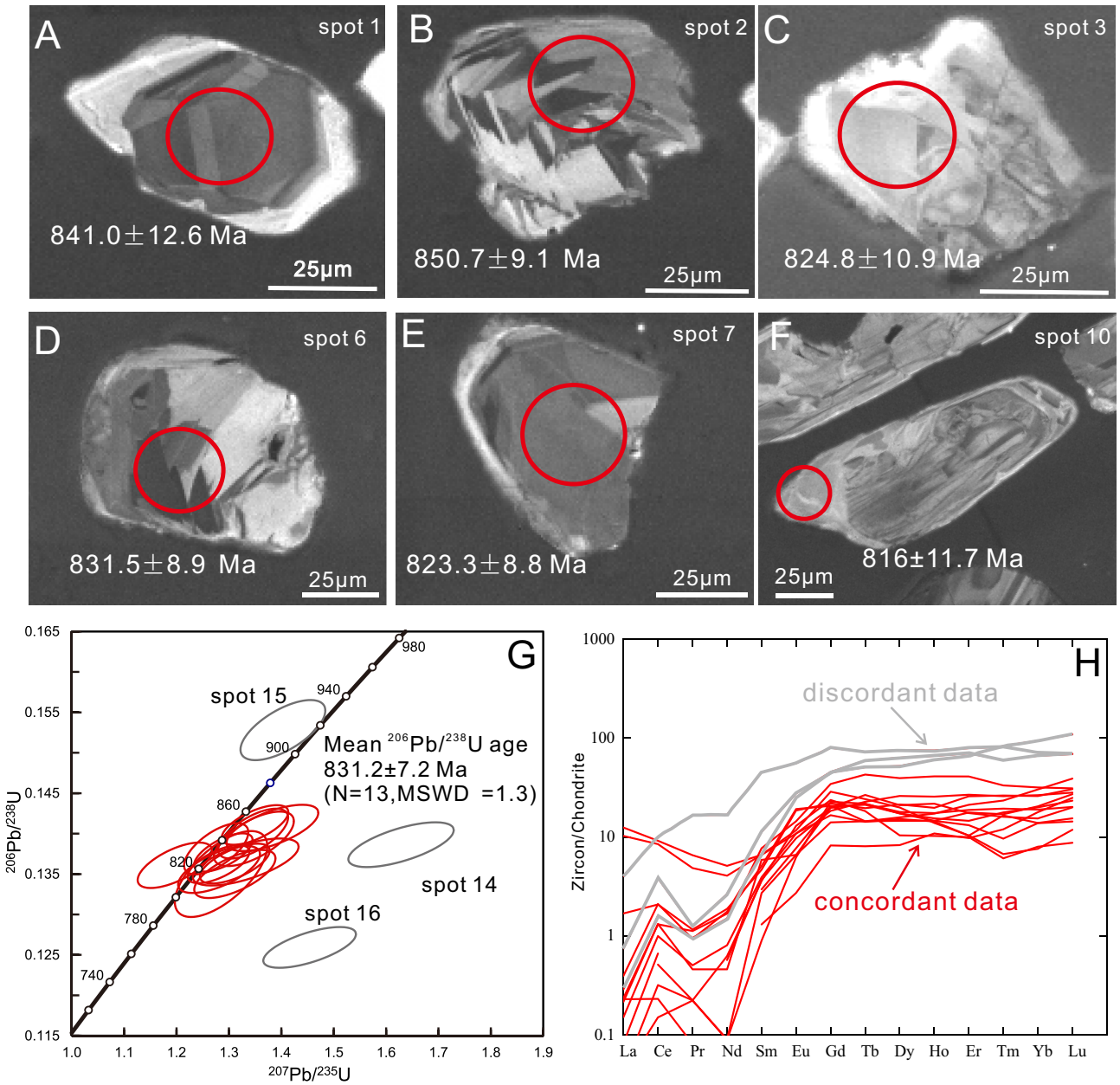

Fig. 5 **A–F** Cathodoluminescence (CL) images of zircon grains from sample 22LC–8, showing the analytical spots and ralated ages (Ma). **G** U–Pb concordia diagram. **H** Chondrite-normalized REE patterns of zircons

5 Discussion

5.1 Timing of metamorphism

The garnet-biotite schist sample 22LC–8 analyzed in this study exhibits zircon characteristics (rounded, patchy, or structureless) with low Th/U ratios (0.003–0.053), which indicate that they are metamorphic zircons (Wu and Zheng 2004). These zircons recorded a weighted mean $^{206}Pb/^{238}U$ age of 831.2 ± 7.2 Ma, which is similar to the metamorphic ages of the garnet muscovite-plagioclase quartz schists and garnet amphibolites from the southwestern margin of the Yangtze Block (Yang et al. 2012, 2013; Li et al. 2021, 2022). The flat to depleted HREE pattern in zircons suggests that they coexisted with garnet during the growth process. The Ti-in-zircon thermometer has yielded the mean temperature of 616 °C, which is lower than the peak metamorphic temperature. Consequently, this age is interpreted to represent the post-peak metamorphic age of the garnet-biotite schist.

In the past decades, geochronological studies of metamorphic rocks from Dahongshan, Yuanmou, Yanbian, and Miyi in the southwestern margin of the Yangtze Block

Table 2 Summary of metamorphic ages in the southwestern margin of the Yangtze Block

Area	Rock Type	Age (Ma)	Minerals (Method)	Reference
Dahongshan Group	Muscovite schist	730	Whole-rock K–Ar	Cao (1997)
Dahongshan Group	Albites	812	Whole-rock K–Ar	Cao (1997)
Dahongshan Group	Biotite schist	706	Whole-rock K–Ar	Cao (1997)
Dahongshan Group	Porphyrite	897	Whole-rock Rb–Sr	Cao (1997)
Dahongshan Group	Marble	808	Biotite K–Ar	Cao (1997)
Dahongshan Group	Marble	819	Biotite K–Ar	Cao (1997)
Dahongshan Group	Schist	818	Sericite K–Ar	Cao (1997)
Dahongshan Group	Marble	800	Biotite K–Ar	Cao (1997)
Dahongshan Group	Amphibolites	860–820	Biotite ^{40}Ar–^{39}Ar	Greentree and Li (2008)
Dahongshan Group	Garnet-amphibolites	849 ± 12	Zircon LA–ICP–MS	Yang et al. (2012)
Dahongshan Group	Garnet-muscovite-plagioclase-quartz schists	837.7 ± 4.2	Muscovite ^{40}Ar–^{39}Ar U–Pb	Yang et al. (2013)
Dahongshan Group	Garnet-muscovite-plagioclase-quartz schists	839.6 ± 4.2	Muscovite ^{40}Ar–^{39}Ar	Yang et al. (2013)
Dahongshan Group	Garne-muscovite-plagioclase-quartz schists	844.2 ± 4.2	Muscovite ^{40}Ar–^{39}Ar	Yang et al. (2013)
Dahongshan Group	Amphibolite	831 ± 20	Amphibole ^{40}Ar–^{39}Ar	Zhou et al. (2014)
Dahongshan Group	Garnet-biotite schist	851 ± 9	Biotite ^{40}Ar–^{39}Ar	Zhou et al. (2014)
Dahongshan Group	Metamorphic gabbros	748.9 ± 5.7	Zircon LA–ICP–MS U–Pb	Jin et al. (2017)
Yuanmou,	Kyanite-bearing garnet staurolite mica schist	885 ± 3	Monazite LA–ICP–MS U–Pb	Li et al. (2021)
Yanbian,	Kyanite-bearing garnet biotite plagioclase gneiss	778 ± 4	Monazite LA–ICP–MS U–Pb	Li et al. (2021)
Miyi	Garnet-bearing sillimanite biotite schist	840 ± 3	Monazite LA–ICP–MS U–Pb	Li et al. (2021)
Yuanmou	Garnet mica schist	767 ± 10	Zircon SHRIMP U–Pb	Li et al. (2022)
Yuanmou	Kyanite-bearing garnet staurolite mica schist	875 ± 9	Zircon SHRIMP U–Pb	Li et al. (2022)
Yuanmou	Kyanite-staurolite-bearing garnet mica schist	882 ± 9	Zircon SHRIMP U–Pb	Li et al. (2022)
Yuanmou	Garnet amphibolite	834 ± 15	Titanite LA–ICP–MS U–Pb	Li et al. (2022)

(Fig. 1B), have yielded metamorphic ages from ca. 885 to 767 Ma, with a peak age at ca. 840 Ma (Cao 1997; Greentree et al. 2006; Yang et al. 2012, 2013; Zhou et al. 2014; Jin et al. 2017; Li et al. 2021, 2022). Similar metamorphic ages have also been obtained from the quartz-carbonate veins of Xikuangshan, Yinachang, and Lala (Zhou et al. 2014). The ages of 860–820 Ma are interpreted as cooling or reset ages subsequent to the Neoproterozoic thermal event (Greentree and Li 2008; Zhou et al. 2014). In contrast, Yang et al. (2012, 2013) and Li et al. (2021, 2022) have proposed that the western margin of the Yangtze Block experienced a period of regional metamorphism during the Neoproterozoic era. As the metamorphic ages reported in the region spread from ca. 885 to 767 Ma (Table 2), supporting that the southwestern Yangtze Block underwent regional metamorphism during the Neoproterozoic with a long duration of the metamorphic event.

5.2 Metamorphic evolution and its tectonic implication

Initial studies suggest that the metamorphic grade of the Dahongshan Group only reached the lower amphibolite facies (Qian and Shen 1990; Yang et al. 2014; Geng et al. 2017), but a systematic study on the metamorphic conditions for the Dahongshan Group is still lacking. In this study, the peak metamorphic condition of garnet-biotite schist sample 22LC–8 is constrained to be 8–9 kbar and 635–675 °C by phase equilibrium modeling (Fig. 4A), which is consistent with the mean temperature of 616 °C obtained from the Ti-zircon thermometer. The garnet in the sample preserves a prograde metamorphic profile (decreasing spessartine, increasing pyrope, and initially constant, then rapidly decreasing grossular from core to rim; Fig. 4C), and thus a prograde *P–T* path with heating and compression is defined for sample 22LC–8 on the basis of the changing trends of the X_{Sps}, X_{Grs}, and X_{Prp} in garnet (Fig. 4C). The metamorphic *P–T* conditions of 6.6–7.8 kbar and 539–570 °C were obtained from the compositions of garnet rims and Bt_2 by GBPQ geothermobarometer below the peak metamorphic condition, which may be related to the fact that Bt_2 represents late-stage retrograde growth. The metamorphic *P–T* conditions obtained from the GBPQ geothermobarometer represent retrograde metamorphic conditions. In addition, the partial replacement of rutile by ilmenite (Fig. 2E) suggests that the sample records a decompression path following the peak metamorphic stage. Therefore, a clockwise metamorphic *P–T* path is constructed. Meanwhile, the results also suggest that the metamorphic grade of Dahongshan Group reached medium to high-grade metamorphism.

Previous studies have investigated the metamorphism of the Miyi, Huili, Yuanmou, and Yanbian regions in the western margin of the Yangtze Block (Fig. 1B; Zhang et al. 1987; Wang et al. 1998; Deng et al. 2001; Geng et al. 2008; Li et al. 2021, 2022), both counterclockwise and clockwise *P–T* paths have been proposed (Fig. 6). Zhang et al. (1987) proposed that the Miyi metamorphic terrane has

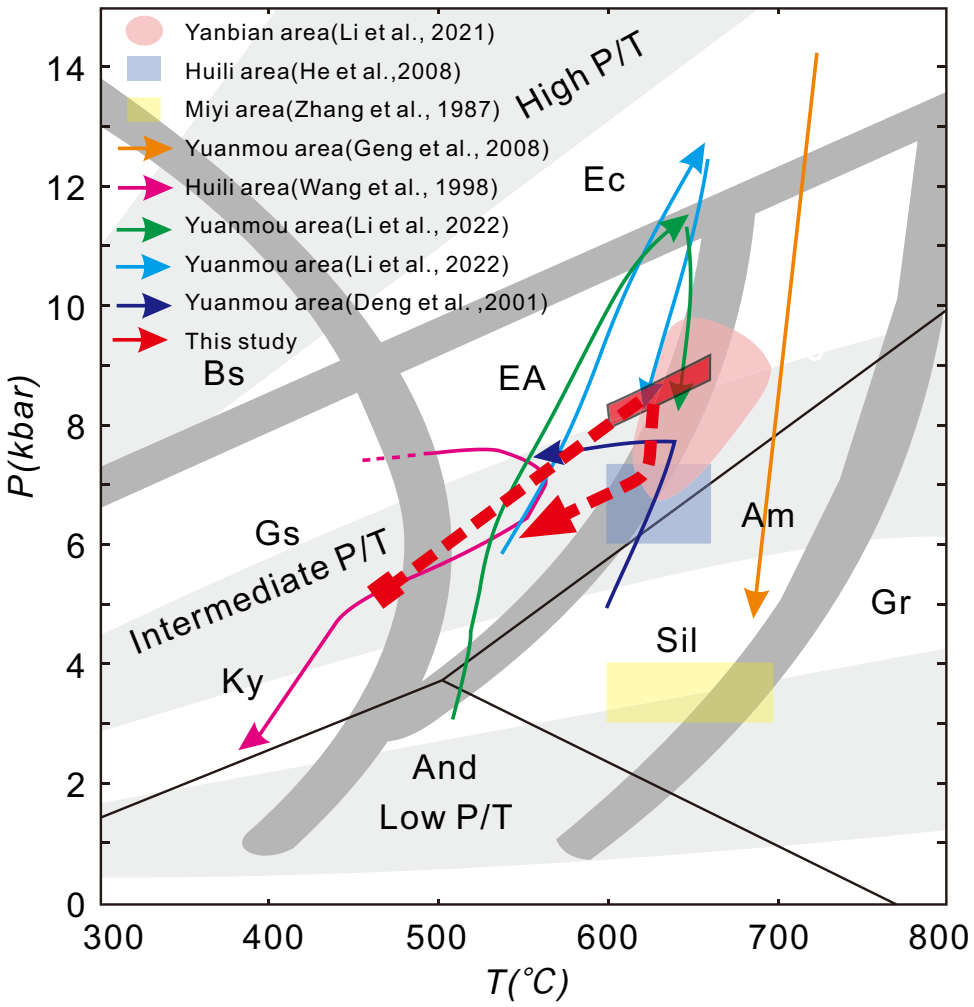

Fig. 6 Metamorphic *P–T* data in the southwestern margin of the Yangtze Block**.** Metamorphic facies and metamorphic facies series are obtained from O'Brien and Rotzler (2003) and Spear (1993), respectively. The Al_2SiO_5 phase transition lines are based on Holdaway and Mukhopadhyay (1993). Gs–greenschist facies; EA–epidote amphibolite facies; Am–amphibolite facies; Gr–granulite facies; Bs–blueschist facies; Ec–eclogite facies; low P/T–low P/T facies series; intermediate P/T–intermediate P/T facies series; high P/T–high P/T facies series

experienced low-pressure metamorphism with conditions of 3.0–4.0 kbar and 600–700 °C (Fig. 6) based on the mineral assemblage of regional metamorphic rocks. Wang et al. (1998) demonstrated that the Xiaoqingshan Formation in the Huili area underwent low- to medium-pressure metamorphism and exhibited a clockwise *P–T* path. In contrast, Deng et al. (2001) conducted a study on the metapelites and metabasites in the Yuanmou area, determining that these rocks underwent a counterclockwise *P–T* path, with peak conditions of 5.9–6.1 kbar and 577–587 °C (Fig. 6). The counterclockwise *P–T* path for the metapelites and metabasites at the Yuanmou area was constrained on the basis of the inference that the absence of retrograde assemblages and no clues of kyanite turning into sillimanite (Deng et al. 2001). Deng et al. (2001) postulated that the counterclockwise *P–T* path in the region may be attributed to contact metamorphism induced by arc magmatism, which is consistent with the conjecture that the Neoproterozoic metamorphism of the southwestern margin of the Yangtze Block is closely related to contemporaneous magmatic activities, as evidenced by the synchronous metamorphic and magmatic events identified along the western margin of the Yangtze Craton (Fan et al. 2020). However, the inference conflicts with the petrographic characteristics (i.e., the symplectite composed of amphibole, and plagioclase around the garnet) of mica schists and garnet amphibolites in the region (Geng et al. 2008; Li et al. 2022). Meanwhile, recent studies have demonstrated that the garnet mica schist, metapelites and garnet amphibolites of the Yuanmou, Yanbian, and Miyi regions in the western margin of the Yangtze Block record a clockwise *P–T* path (Li et al. 2021, 2022). The clockwise *P–T* path involves a near-isothermal decompressional process, and is widely acknowledged as indicative of continental collision dynamics (England and Thompson 1984; Thompson and England 1984). Therefore, the metamorphic rocks in the western margin of the Yangtze Block all record a clockwise *P–T* path, suggesting that the formation of these metamorphic rocks is related to the collisional orogenic process. This could be associated with the late-stage assembly of the Rodinia supercontinent, or localized compression and subduction events that occurred during the breakup of the Rodinia supercontinent (Geng et al. 2008). In addition, the

peak metamorphic *P–T* conditions of the metamorphic rocks from different locations within the southwestern margin of the Yangtze Block are diverse, which indicates that these rocks were possibly buried to diverse depths and thus record different metamorphic conditions in orogenic belts (Wang et al. 2017).

6 Conclusions

1. The garnet-biotite schist from the Dahongshan Group recorded a clockwise *P–T* path, with peak metamorphic conditions of 8–9 kbar and 635–675 °C.
2. The post-peak metamorphic age of the garnet-biotite schist from the Dahongshan Group is 831.2 ± 7.2 Ma.
3. Neoproterozoic metamorphism along the western margin of the Yangtze Block is related to collisional orogenesis, possibly reflected by either the late-stage assembly of the Rodinia supercontinent or localized compression and subduction concurrent with the breakup of the Rodinia supercontinent.

Acknowledgements We appreciate our editor Dr. Binbin Wang, and three anonymous reviewers for their constructive comments that significantly improve this paper. This work was financially supported by the National Natural Science Foundation of China (Grant Nos. 42162012, 42072094) and the Key Laboratory of Sanjiang Metallogeny and Resource Exploration and Utilization, Ministry of Natural Resources (Project No. ZRZYBSJSYS2022001).

Author contributions Jun-xiao Ma: Data curation, Funding acquisition, Investigation, Methodology, Writing-original draft; Guang-shu Yang, Yong-feng Yan, Xiao-Fei Xu: Funding acquisition, Investigation, Supervision, Writing-review & editing; Yun-hua Ren, Hui Zhao, Xiao-jun Zheng, Yuan Qin: Data curation, Investigation.

Declarations

Conflict of interest We declare no conflicts of interest in this study.

Ethical approval All authors have approved the manuscript and agree with its submission.

References

Ague JJ, Carlson WD (2013) Metamorphism as garnet sees it: The kinetics of nucleation and growth, equilibration, and diffusional relaxation. Elements. 9:439–445.

Caddick MJ, Kohn MJ (2013) Garnet: Common mineral, uncommonly useful. Elements. 9:415–419.

Cao DB (1997) Metamorphism characteristics of Dahongshan rock group in the Nangan-Xilahe area. Yunnan Geol. 16:184–191 (**in Chinese with English abstract**).

Chen YL, Luo ZH, Zhao JX, Li ZH, Zhang HF, Song B (2005) Petrogenesis and dating of the Kangding complex, Sichuan Province. Sci China Ser D Earth Sci. 48:622–634.

Deng SX, Wang JH, Zhu BQ (2001) PTt path of metamorphism for the Julin Group and its geodynamical implications in Yuanmou, Yunnan. Sci China, Ser D Earth Sci. 44:609–620.

Du LL, Guo JH, Geng YS, Yang CH, Liu FL, Ren LD, Liu PH (2013) Age and tectonic setting of the Yanbian Group in the southwestern Yangtze Block: Constraints from clastic sedimentary rocks. Acta Petrol Sinica. 29:641–672 (**in Chinese with English abstract**).

England PC, Thompson AB (1984) Pressure–temperature–time paths of regional metamorphism I. Heat transfer during the evolution of regions of thickened continental crust. J Petrol. 25:894–928.

Fan HP, Zhu WG, Li ZX (2020) Paleo- to Mesoproterozoic magmatic and tectonic evolution of the southwestern Yangtze Block, south China: New constraints from ca. 1.7–1.5 Ga mafic rocks in the Huili-Dongchuan area. Gondwana Res. 87:248–262.

Geng YS, Liu YQ, Gao LZ, Peng N, Jiang XJ (2012) Geochronology of the Mesoproterozoic Tong'an Formation in southwestern margin of Yangtze craton: New evidence from zircon LA-ICP-MS U-Pb ages. Acta Petrol Sinica. 86:1479–1490 (**in Chinese with English abstract**).

Geng YS, Kuang HW, Liu YQ, Du LL (2017) Subdivision and correlation of the mesoproterozoic stratigraphy in the Western and Northern Margins of Yangtze Block. Chin Acad Geol Sci. 91:2151–2174 (**in Chinese with English abstract**).

Geng YS, Yang CH, Wang XS, Du LL, Ren LD, Zhou XW (2008) Metamorphic basement evolution in western margin of Yangtze Block. Geological Publishing House, Beiing, vol 1, p 215 (**in Chinese with English abstract**).

Geng YS (2015) Neoproterozoic era of south China Craton. Precambrian Geol China, pp 263–301.

Greentree MR, Li ZX (2008) The oldest known rocks in south–western China: SHRIMP U-Pb magmatic crystallisation age and detrital provenance analysis of the Paleoproterozoic Dahongshan Group. J Asian Earth Sci. 33:289–302.

Greentree MR, Li ZX, Li XH, Wu H (2006) Late Mesoproterozoic to earliest Neoproterozoic basin record of the Sibao orogenesis in western South China and relationship to the assembly of Rodinia. Precambr Res. 151:79–100.

Henry DJ, Guidotti CV, Thomson JA (2005) The Ti-saturation surface for low-to-medium pressure metapelitic biotites: Implications for geothermometry and Ti-substitution mechanisms. Am Miner. 90:316–328.

Holdaway MJ, Mukhopadhyay B (1993) A reevaluation of the stability relations of andalusite: thermochemical data and phase diagram for the aluminum silicates. Am Mineral. 78:298–315.

Holland TJB, Powell R (1998) An internally consistent thermodynamic data set for phases of petrological interest. J Metamorph Geol. 16:309–343.

Holland T, Powell R (2003) Activity–composition relations for phases in petrological calculations: An asymmetric multicomponent formulation. Contrib Miner Petrol. 145:492–501.

Holland TJB, Powell R (2011) An improved and extended internally consistent thermodynamic dataset for phases of petrological interest, involving a new equation of state for solids. J Metamorph Geol. 29:333–383.

Huang XL, Xu YG, Li XH, Li WX, Lan JB, Zhang HH, Yang QJ (2008) Petrogenesis and tectonic implications of Neoproterozoic, highly fractionated A–type granites from Mianning, South China. Precambrian Res. 165:190–204.

Jin TF, Li YG, Fei GC, Feng YC, Zhou H, Sha XB, Wu K (2017) Geochronology of zircon U-Pb from Hongshan formation in the Dahongshan Group in the Southwest Yangtze Block for the

Redefinitions of the forming age of the protolith and metamorphic age. Geol Rev. 63:894–910.
Li ZX, Li X, Kinny P, Wang J, Zhang S, Zhou H (2003) Geochronology of Neoproterozoic syn-rift magmatism in the Yangtze Craton, South China and correlations with other continents: Evidence for a mantle superplume that broke up Rodinia. Precambr Res. 122:85–109.
Li ZM, Chen Y, Zhang QW, Liu JH, Wu CM (2021) U-Pb dating of metamorphic monazite of the Neoproterozoic Kang-Dian Orogenic Belt, southwestern China. Precambr Res. 361:106262.
Li ZM, Chen Y, Zhang QW, Liu JH, Wu CM (2022) PT conditions and timing of metamorphism of the Yuanmou area, southern Neoproterozoic Kang-Dian Orogenic Belt, southwest China. Precambr Res. 374:106642.
Liu WZ, Xu SJ, Wang RC, Zhao LZ, Li HM, Wu JQ, Fang Z (2005) Zircon U-Pb geochronology of granulites in Panzhihua-Xichang area: New evidence for the Neoproterozoic geological evolution in the Western margin of Yangtze Block. Geol Rev. 51:470–476.
Liu Y, Hu Z, Gao S, Günther D, Xu J, Gao C, Chen H (2008) *In-situ* analysis of major and trace elements of anhydrous minerals by LA-ICP-MS without applying an internal standard. Chem Geol. 257:34–43.
Liu Y, Gao S, Hu Z, Gao C, Zong K, Wang D (2010) Continental and oceanic crust recycling-induced melt–peridotite interactions in the Trans-North China Orogen: U-Pb dating, Hf isotopes and trace elements in zircons from mantle xenoliths. J Petrol. 51:537–571.
Ludwig KR (2003) ISOPLOT 3.00: A geochronological toolkit for microsoft excel (Berkeley Geochronology Center, Berkeley, California). Berkeley: BGC Special Publishing.
Munteanu M, Wilson A, Yao Y, Harris C, Chunnett G, Luo Y (2010) The Tongde dioritic pluton (Sichuan, SW China) and its geotectonic setting: regional implications of a local-scale study. Gondwana Res. 18:455–465.
O'Brien PJ, Rötzler J (2003) High-pressure granulites: Formation recovery of peak conditions and implications for tectonics Abst J Metamorph Geol. 21(1):3–20. https://doi.org/10.1046/j.1525-1314.2003.00420.x
Pang WH, Ren GM, Sun ZM, Yin FG (2015) Division and correlation of Paleo-Mesoproterozoic strata on the western margin of Yangtze block: Evidence from the U-Pb age of tuff zircon in the Tongan Formation. Geol China. 42:921–936.
Qian JH, Shen YR (1990) The Dahongshan volcanogenic Fe-Cu deposit in Yunnan Province. Series of geological memoirs of People's Republic of China. 236 (**in Chinese with English abstract**).
Spear FS (1993) Metamorphic phase equilibria and pressure-temperature-time paths. Mineralogical Society of America monograph. Washington, D.C.
Thompson AB, England PC (1984) Pressure-temperature-time paths of regional metamorphism II. Their inference and interpretation using mineral assemblages in metamorphic rocks. J Petrol. 25:929–955.
Wang JZ, Lu Y, Xiao YF, Wen CQ (1998) Metamorphic Petrology and PTD Path of Xiaoqingshan Formation in the Xiaoqingshan Cu(Au) Deposit, Huili County, Sichuan Province. Acta Petrol Mineral. 17:216–225 (**in Chinese with English abstract**).
Wang XC, Li XH, Li WX, Li ZX (2007) Ca. 825 Ma komatiitic basalts in South China: First evidence for >1500 °C mantle melts by a Rodinian mantle plume. Geology. 35:1103–1106.
Wang H, Chen YC, Zhang HX, Shi MY, Yan QR, Hou QL, Zhang Q, Kusky T, Wu CM (2017) Tectonic m´elange records the Silurian-Devonian subduction-metamorphic process of the southern Dunhuang terrane, southernmost Central Asian Orogenic Belt. Geology. 45:427–430.
White RW, Powell R (2002) Melt loss and the preservation of granulite facies mineral assemblages. J Metamorph Geol 20:621–632
White R, Powell R, Holland T, Johnson T, Green E (2014) New mineral activity–composition relations for thermodynamic calculations in metapelitic systems. J Metamorph Geol. 32:261–286.
Whitney DL, Evans BW (2010) Abbreviations for names of rock-forming minerals. American Mineralogis. 95:185–187.
Wu CM, Zhang J, Ren LD (2004) Empirical garnet–biotite–plagioclase–quartz (GBPQ) geobarometry in medium-to high-grade metapelites. J Petrol. 45:1907–1921.
Xiang H, Connolly JAD (2022) GeoPS: An interactive visual computing tool for thermodynamic modelling of phase equilibria. Abstract J Metamorphic Geol. 40(2):243–255. https://doi.org/10.1111/jmg.v40.2 10.1111/jmg.12626
Xiao L, Zhang HF, Ni PZ, Xiang H, Liu XM (2007) LA-ICP-MS U-Pb zircon geochronology of early Neoproterozoic mafic-intermediat intrusions from NW margin of the Yangtze Block, South China: Implication for tectonic evolution. Precambr Res. 154:221–235.
Yan YB (1981) On the ore-bearing rock mass in Dahongshan, Yunnan Province. J Kunming Inst Technol. 2:20–28.
Yang H, Liu FL, Du LL, Liu PH, Wang F (2012) Zircon U-Pb dating for metavolcanites in the Laochanghe Formation of the Dahongshan Group in southwestern Yangtze Block, and its geological significance. Acta Petrol Sinica. 28:2994–3014 (**in Chinese with English abstract**).
Yang H, Liu FL, Liu PH, Wang F (2013) ^{40}Ar–^{39}Ar dating for muscovite in garnet muscovite-felsic schists of the Dahongshan Group in southwestern Yangtze Block and its geological significance. Acta Petrol Sinica. 29:2161–2170 (**in Chinese with English abstract**).
Yang H, Liu PH, Meng E, Wang F, Xiao LL, Liu CH (2014) Geochemistry and its tectonic implications of metabasite in the Dahongshan Group in southwestern Yangtze block. Acta Petrol Sinica. 30:3021–3033 (**in Chinese with English abstract**).
Zhang RY, Cong BL, Wang MK (1987) A preliminary research on Precambrian low-pressure metamorphic terrain in the Miyi, Sichuan Province. Acta Petrol Sinica. 3:3–13.
Zhang G, Guo A, Wang Y, Li S, Dong Y, Liu S, Yao A (2013) Tectonics of South China continent and its implications. Sci China Earth Sci. 56:1804–1828.
Zhao G (2015) Jiangnan Orogen in South China: Developing from divergent double subduction. Gondwana Res. 27:1173–1180.
Zhou MF, Yan DP, Kennedy AK, Li Y, Ding J (2002) SHRIMP U-Pb zircon geochronological and geochemical evidence for Neoproterozoic arc-magmatism along the western margin of the Yangtze Block, South China. Earth Planet Sci Lett. 196:51–67.
Zhou MF, Zhao XF, Chen TW, Li XC, Wang W, Yan DP, Qiu HN (2014) Proterozoic Fe–Cu metallogeny and supercontinental cycles of the southwestern Yangtze Block southern China and northern Vietnam. Earth Sci Rev. https://doi.org/10.1016/j.earscirev.2014.08.013
Zhu WG, Zhong H, Li XH, Deng HL, He DF, Wu KW, Bai ZJ (2008) SHRIMP zircon U-Pb geochronology, elemental, and Nd isotopic geochemistry of the Neoproterozoic mafic dykes in the Yanbian area, SW China. Precambrian Res. 164:66–85.